

# Spectroscopy and Infrared Photofragmentation

## Dynamics of Mixed Ligand Ion-Molecule

### Complexes: $\text{Au}(\text{CO})_x(\text{N}_2\text{O})_y^+$

*Alice E. Green, Rachael H. Brown, Gabriele Meizyte, and Stuart R. Mackenzie\**

Department of Chemistry, University of Oxford, Physical and Theoretical Chemistry

Laboratory, South Parks Road, Oxford, United Kingdom, OX1 3QZ

\*stuart.mackenzie@chem.ox.ac.uk

## **Supporting Information**

# Table of Contents

|  |    |
|--|----|
| Table of Contents  | 2  |
| A. Experimental Details  | 3  |
| <b>Figure S1.</b>  | 3  |
| B. Computational Details   | 4  |
| C. Infrared Spectra of $\text{Au}(\text{CO})_x(\text{N}_2\text{O})_y^+$ Complexes: Simulated   | 6  |
| <b>Figure S2.</b>  | 6  |
| <b>Figure S3.</b>  | 7  |
| <b>Figure S4.</b>  | 8  |
| <b>Figure S5.</b>  | 9  |
| D. Infrared Spectra of $\text{Au}(\text{CO})_x(\text{N}_2\text{O})_y^+$ Complexes: Assignments | 10 |
| <b>Table S1.</b>   | 10 |
| <b>Figure S6.</b>  | 11 |
| <b>Figure S7.</b>  | 12 |
| <b>Figure S8.</b>  | 13 |
| <b>Figure S9.</b>  | 15 |
| E. Photofragmentation Dynamics and Branching Ratios  | 16 |
| <b>Figure S10.</b>   | 16 |
| <b>Figure S11.</b>   | 17 |
| <b>Figure S12.</b>   | 18 |
| F. Calculated Internal Energy Distributions and Dissociation Thresholds                        | 19 |
| <b>Figure S13.</b>   | 19 |
| G. Effects of Multiple Photon Absorption   | 20 |
| <b>Figure S14.</b>   | 20 |
| <b>Figure S15.</b>   | 21 |
| H. References:   | 22 |

## A. Experimental Details

Typical rf only (i.e., total) mass spectrum together with the effects of mass selection and photofragmentation. The quadrupole mass filter is effective in isolating individual parent ion-molecule complexes of interest and photofragmentation spectra are then recorded against a zero background, enhancing the signal to noise achieved.

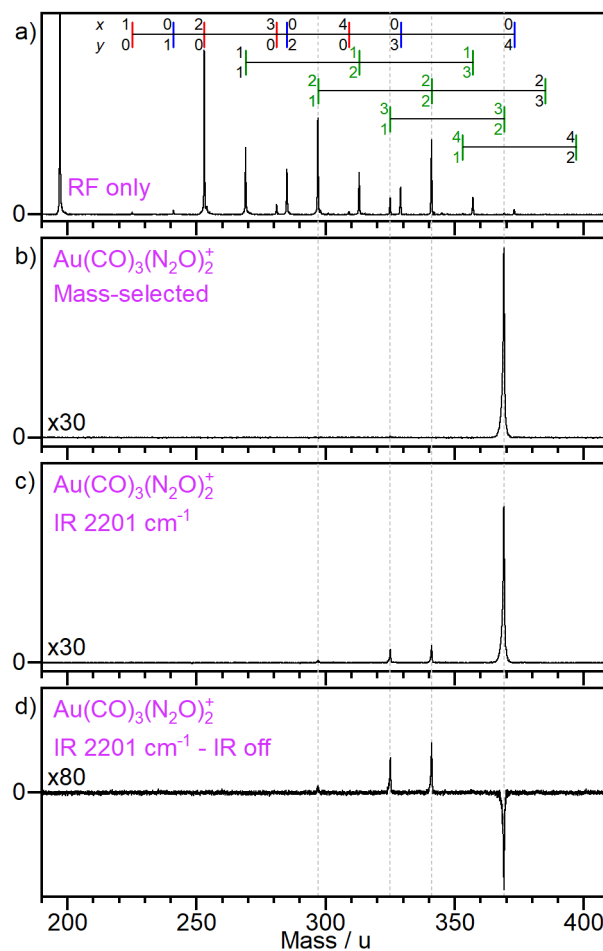


**Figure S1.** Time-of-flight mass spectra showing: a) Typical distribution of  $\text{Au}(\text{CO})_x(\text{N}_2\text{O})_y^+$  complexes obtained with mass filtering disabled. Different species types are indicated by red ( $y = 0$ ), blue ( $x = 0$ ) and green ( $x$  and  $y > 0$ ) lines with green numbers highlighting the species investigated in the following sections. In b)-d) mass selection is enabled at the mass corresponding to  $\text{Au}(\text{CO})_3(\text{N}_2\text{O})_2^+$ .

## B. Computational Details

To assist in assignment of the experimental spectra, IRPD spectra have been compared with the simulated spectra of energetically low-lying structures of mixed ligand clusters from density functional theory (DFT). The structure search was performed using a large range of chemically intuitive starting structures, in addition to the stochastic KICK algorithm developed by Addicoat and Metha.<sup>1</sup> A range of functionals and basis sets was employed, with comparisons shown below (Section C) for the representative B3P86-Def2TZVP functional-basis set combination.<sup>2-5</sup> Scalar relativistic effects were included *via* the use of the Stuttgart Dresden effective core potential (ECP60 for gold atoms).<sup>6</sup> Use of the TPSS<sup>7-8</sup> functional and further inclusion of dispersion parameters<sup>9-10</sup> made no qualitative difference to the relative energy ordering of key structures. All structures and spectra presented are in the singlet state with corresponding triplet structures lying > 3 eV higher in energy.

The following notation to explain the core structure type will be used throughout Section C and is given to the right of each simulated spectrum (*i.e.*, a key for the ligands bound directly to Au<sup>+</sup>):

1. Text colour - the identity of molecules in the core shell (also given by the figure key: CO = red, N<sub>2</sub>O = dark blue, N<sub>2</sub> = light blue and CO<sub>2</sub> = orange),
2. Letter - the element symbol of the atom the molecule is bound to the metal through (e.g., C = C-bound CO, N = terminal N-bound N<sub>2</sub>O and O = either O-bound CO or N<sub>2</sub>O),
3. Superscript - the number of molecules in the core bound in that way.

In each case, only the lowest energy of each core structure type is given. The structures with the same core structure definition but with slight differences in geometry present very similar simulated spectra. Furthermore, the spectra are most diagnostic of the core structure, and once ligands are not directly bound to the metal centre their vibrations appear close to those of free molecules. The binding mode of either a CO or N<sub>2</sub>O molecule outside the core has negligible effect on the energy of the cluster. The outer shell N<sub>2</sub>O stretch, irrespective of binding mode, lies close to the inner O-bound at 2230-2240 cm<sup>-1</sup>. The outer O-bound CO is out of the range of our spectrum, but the outer C-bound CO band, although significantly less blue shifted from its core frequency, presents a low intensity band at 2170-2180 cm<sup>-1</sup>, which there is no sign of in the experimental spectra. This is an additional piece of evidence supporting the assignment of the lowest energy structures which have no CO molecules outside the core shell.

All energies are zero point corrected and relative to the lowest energy Au(CO)<sub>x</sub>(N<sub>2</sub>O)<sub>y</sub><sup>+</sup> structure for each combination of *x* and *y*. All simulated spectra have been convoluted with a Lorentzian function with a 8 cm<sup>-1</sup> full width half maximum (FWHM) to match experimental linewidths and intensities are given as  $\epsilon$ , the molar absorption coefficient. Using the same key as Part 1 above, the molecular assignments of the vibrations are indicated by the coloured lines with heights equivalent to the maxima of individual vibrations.

Experimental spectra are shown as the sum of all fragment channel enhancements and are not on the same scale. Dashed lines indicate the C≡O stretch (2143.2 cm<sup>-1</sup>) and N=N stretch (2223.5 cm<sup>-1</sup>) in free CO and N<sub>2</sub>O, respectively, and use the same colour scheme as Part 1 of the key.<sup>11-12</sup>

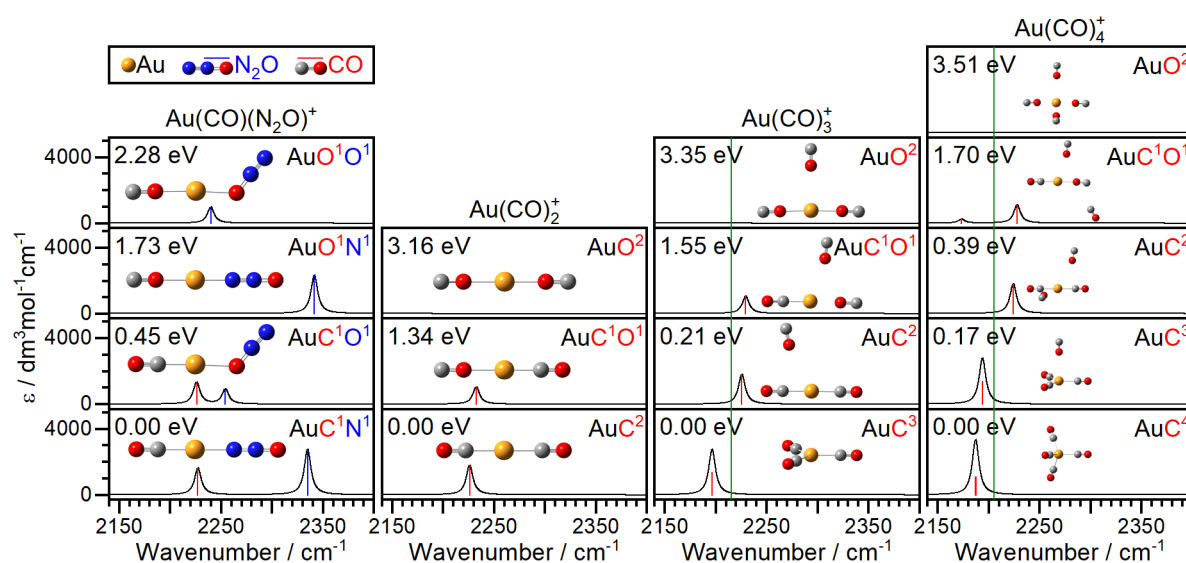
Traditionally, for comparison with IR action spectra, DFT simulated IR spectra are scaled to the frequency of the free molecule in question and these errors in the simulated vibrational frequencies can be attributed to both the use of harmonic potentials and the inadequacies of the method to explain electron correlation in the structure calculation.<sup>13</sup> In this paper, however, N<sub>2</sub>O and CO have very different scaling factors and at this level of theory (B3P86-Def2TZVP) they are 0.932 and 0.963, respectively. Anharmonic calculations bring the scaling factors closer to one but are insufficient to explain the error alone. In this case a compromise must be made and the N<sub>2</sub>O modes are scaled by the N=N stretching frequency, whereas the CO modes are scaled by the C≡O stretching frequency. It is important to note that this only works for strictly local modes that involve relative C to O or N to N displacements within a CO or N<sub>2</sub>O molecule. For example, it is unphysical to describe any intermolecular modes, such as an Au-C stretch, in this way. Fortunately, only the N=N stretch of N<sub>2</sub>O and C≡O stretch of CO are probed within the spectral range here.

All IRPD spectra show reasonable agreement with simulated spectra of the lowest energy calculated cluster (See Figures S2-5 below).

## C. Infrared Spectra of $\text{Au}(\text{CO})_x(\text{N}_2\text{O})_y^+$ Complexes: Simulated

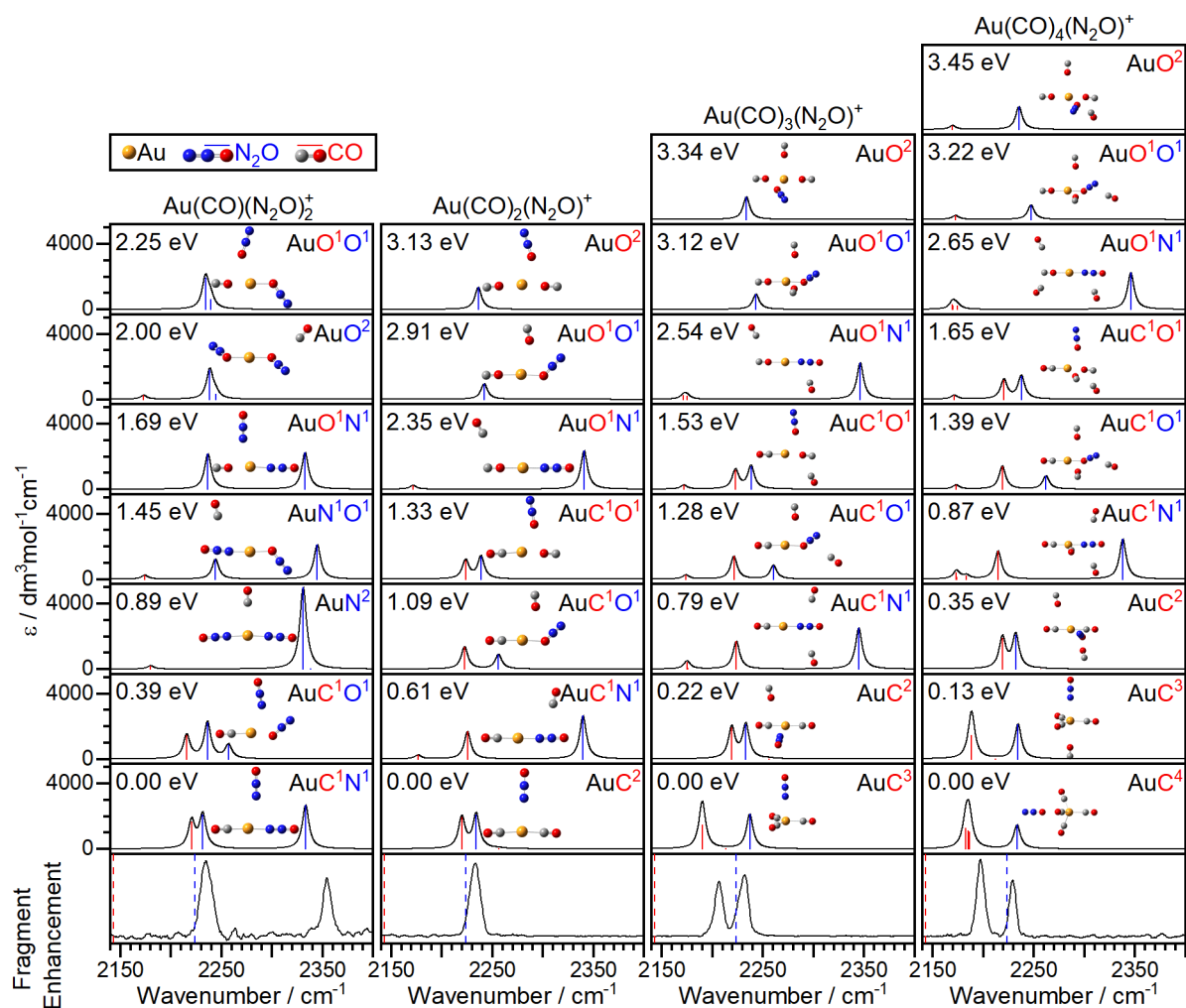
This Section contains more extensive data similar to that shown in Figure 4 comparing experimental IR spectra with simulated spectra.

Figure S2 shows the calculated IR spectra of complexes which were not observed in this study due to either low number density in the molecular beam and/ or binding energies which preclude efficient infrared dissociation but also because the study concentrated on mixed ligand complexes. They represent the core structures to which all the mixed ligand complexes are built on.



**Figure S2.** Simulated IR spectra of energetically low-lying isomers of  $\text{Au}(\text{CO})_x(\text{N}_2\text{O})_y^+$  ( $x,y = 1;1, 2;0, 3;0, 4;0$ ). The lowest lying isomers exist with all ligands directly bound to the core. The solid green lines indicate the observed experimental peak positions from Duncan and coworkers.<sup>14-15</sup>

Figure S3 - as Figure 4 in the main manuscript but including higher-lying structure types (e.g. O-bound CO) that are very unlikely to be present in the cluster beam.



**Figure S3.** Comparison of IRPD spectra of  $\text{Au}(\text{CO})_x(\text{N}_2\text{O})_y^+$  ( $x,y = 1;2, 2;1, 3;1, 4;1$ ) with the simulated IR spectra of energetically low-lying isomers. The lowest lying isomers exist as a core with one additional outer  $\text{N}_2\text{O}$  ligand.

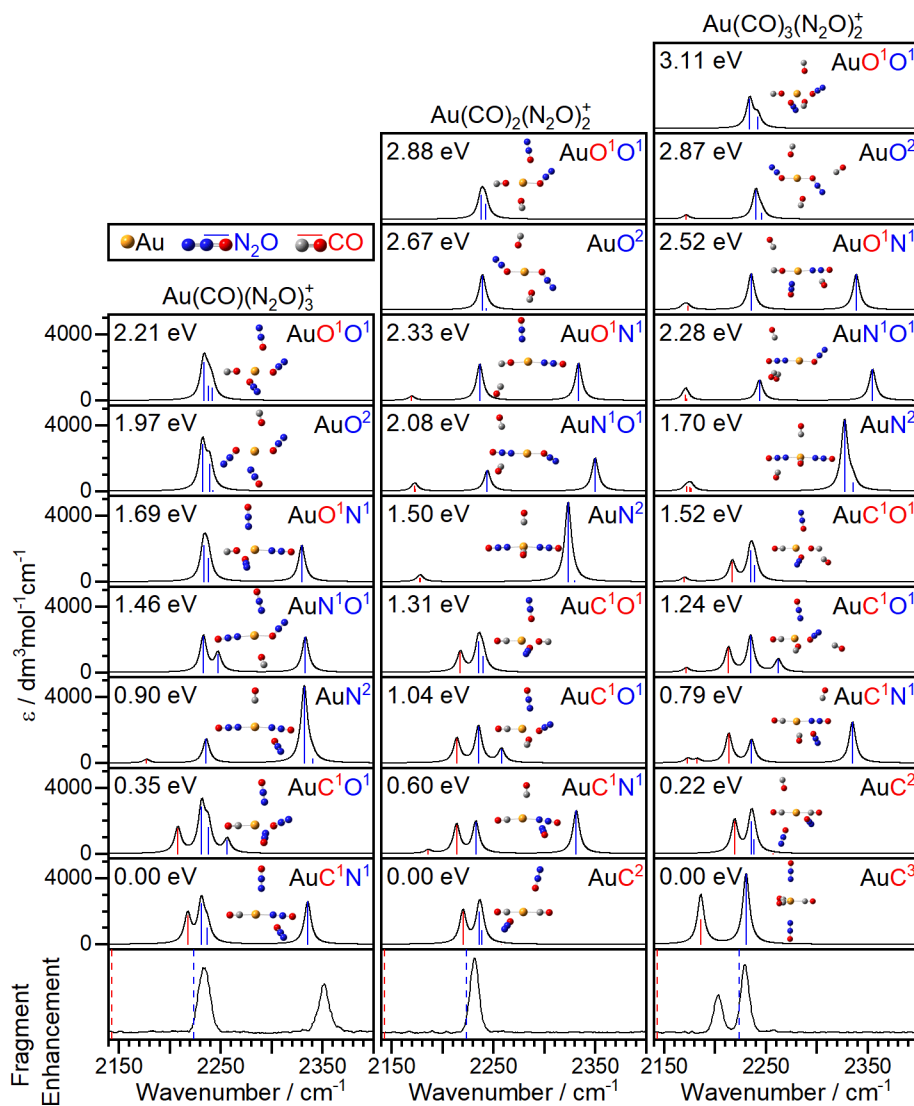


**Figure S4.** Comparison of IRPD spectra of Au(CO)<sub>x</sub>(N<sub>2</sub>O)<sub>y</sub> (x,y = 1;3, 2;2, 3;2) with the simulated IR spectra of energetically low-lying isomers. The lowest lying isomers exist as a core with two additional outer N<sub>2</sub>O ligands.



## Exit-channel complexes

Figure S5 compares experimental spectra with simulated spectra assuming the  $\text{CO} + \text{N}_2\text{O} \rightarrow \text{CO}_2 + \text{N}_2$  reaction has occurred. In reality, the exothermicity of this reaction (indicated) coupled with the low binding energy of the product ligands makes it highly unlikely that such product channel species are observed. In addition, a likely intermediate to these reactions is an oxide such as  $\text{AuO}(\text{CO})(\text{N}_2)^+$  but these are at least 2 eV higher in energy than an unreacted  $\text{Au}(\text{CO})(\text{N}_2\text{O})^+$  species and above the  $\text{Au}^+ + \text{CO} + \text{N}_2\text{O}$  asymptote.

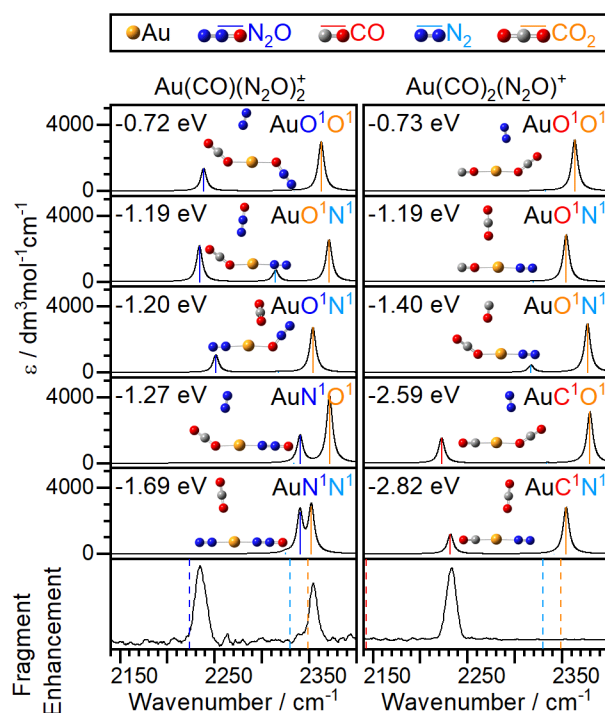
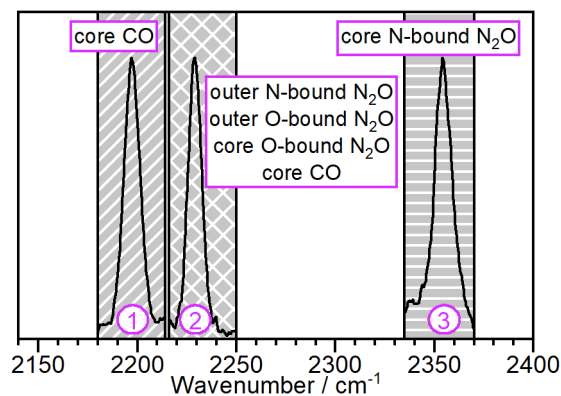


**Figure S5.** Comparison of IRPD spectra of  $\text{Au}(\text{CO})(\text{N}_2\text{O})_2^+$  and  $\text{Au}(\text{CO})_2(\text{N}_2\text{O})^+$  with simulated IR spectra of reacted (exit channel) isomers, in which the redox couple ( $\text{CO} + \text{N}_2\text{O} \rightarrow \text{CO}_2 + \text{N}_2$ ) has completed once. The dashed lines indicate the frequency of the vibrations in the free molecule of the corresponding colour.<sup>11-12</sup>

## D. Infrared Spectra of $\text{Au}(\text{CO})_x(\text{N}_2\text{O})_y^+$ Complexes: Assignments

**Table S1.** Summary of spectral features observed in the IRPD spectra of  $\text{Au}(\text{CO})_x(\text{N}_2\text{O})_y^+$  ( $x = 1-4$ ,  $y = 1-3$ ) complexes. The regions are assigned to types of CO or  $\text{N}_2\text{O}$  stretches. These assignments come from monochromophore studies<sup>15-16</sup> in Figure S6 and DFT simulations in Figures S2-4. See text in main manuscript for details (Section 3.1).



| region<br>/ $\text{cm}^{-1}$ | 1. 2180<br>- 2215 | 2. 2215<br>- 2250 | 3. 2335<br>- 2370 |
|------------------------------|-------------------|-------------------|-------------------|
| $x, y$                       |                   |                   |                   |
| 1 2                          |                   | ✓                 | ✓                 |
| 1 3                          |                   | ✓                 | ✓                 |
| 2 1                          |                   | ✓                 |                   |
| 2 2                          |                   | ✓                 |                   |
| 3 1                          | ✓                 | ✓                 |                   |
| 3 2                          | ✓                 | ✓                 |                   |
| 4 1                          | ✓                 | ✓                 |                   |

## Pure CO / N<sub>2</sub>O complexes

The focus of this manuscript is on the mixed-ligand complexes. Duncan and coworkers<sup>14-15</sup> have studied Au(CO)<sub>n</sub><sup>+</sup> complexes in detail and Cunningham *et al.*<sup>16</sup> have reported the spectra and interpretation of Au(N<sub>2</sub>O)<sub>n</sub><sup>+</sup> complexes.

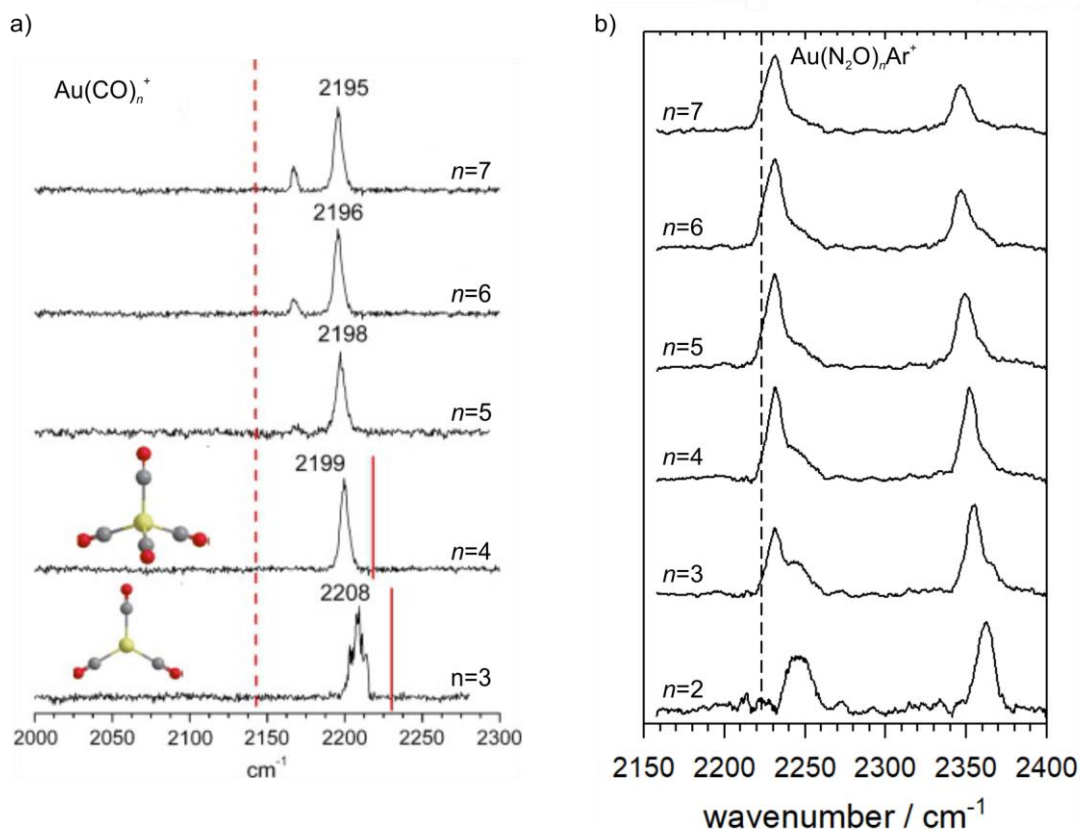


**Figure S6.** IRPD spectra of a) Au(CO)<sub>m</sub><sup>+</sup> (*m* = 3-7) and b) Au(N<sub>2</sub>O)<sub>m</sub>Ar<sup>+</sup> (*m* = 2-7), adapted from Ricks *et al.*,<sup>14</sup> with the permission of Elsevier and from Cunningham *et al.*,<sup>16</sup> copyright 2017 American Chemical Society, respectively. Spectra in a) are recorded as enhancement of daughter fragments and are originally published by Velasquez *et al.*<sup>15</sup> Spectra in b) are recorded using the inert messenger technique. The dashed lines indicate the frequency of vibrations in free CO (2143.2 cm<sup>-1</sup>) and N<sub>2</sub>O (2223.5 cm<sup>-1</sup>).<sup>11-12</sup>

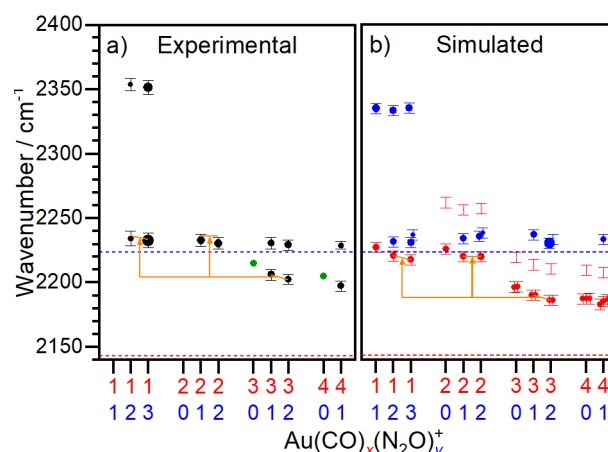


**Figure S7.** a) Experimental peak positions displayed as a function of cluster size for  $\text{Au}(\text{CO})_x(\text{N}_2\text{O})_y^+$  ( $x = 1-4$ ,  $y = 1-3$ ). The uncertainties in the peak positions correspond to the full width half maximum (FWHM) of the fitted peak and the area of the dots is proportional to the area under the fit. The green dots are taken directly from the peak positions of Duncan and coworkers.<sup>14-15</sup> b) The corresponding simulated peak positions and areas of lowest energy isomers, all given a typical  $8 \text{ cm}^{-1}$  FWHM. The colours illustrate the molecular assignments of the vibrations (red =  $\text{C}\equiv\text{O}$  stretch, blue =  $\text{N}=\text{N}$  stretch in  $\text{N}_2\text{O}$ ). In a) and b) orange arrows represent the relative shifts in the simulated  $\text{C}\equiv\text{O}$  band.

Figure S7a shows the frequency of the experimental bands with the uncertainties representing the FWHM of the peaks. From the narrow FWHM ( $9-11 \text{ cm}^{-1}$ ) of the single band at *ca.*  $2230 \text{ cm}^{-1}$  for  $x = 1$  and 2 species, it seems unlikely, but not impossible that it represents more than one different absorption (both  $\text{C}\equiv\text{O}$  and  $\text{N}=\text{N}$ ).

In Figure S7b the  $\text{C}\equiv\text{O}$  band blue shifts further from free CO with decreasing  $x$ . In the gas phase, spectra of  $\text{Au}(\text{CO})^+$  or  $\text{Au}(\text{CO})_2^+$  have not yet been recorded and in the condensed phase their band positions are highly dependent on conditions.<sup>17-20</sup> However, a larger blue shift for  $x = 1$  ( $2236.8 \text{ cm}^{-1}$ ) and 2 ( $2233.4 \text{ cm}^{-1}$ ), compared to  $x = 3$  ( $2203.5 \text{ cm}^{-1}$ ) and 4 ( $2193.5 \text{ cm}^{-1}$ ), was seen in neon matrix experiments,<sup>21</sup> and can be explained by a linear *sd* hybridised orbital on the gold atom creating a stronger ‘non classical’ interaction in  $x = 1$  and 2. This Orgel effect<sup>22</sup> is seen for many  $\text{Au}(\text{L})_2^+$  systems,<sup>16, 23-24</sup> and is responsible for the large abundance of  $\text{Au}(\text{CO})_2^+$  in Figure 2b of the main text. The simulated shifts of  $x = 1$  and 2 relative to  $x = 3$  are given by the orange arrows, and when the  $x = 3$  experimental positions in Figure S7a are overlaid by the same orange arrows, the  $x = 1$  and 2 positions are exactly coincident with the experimental band already assigned to the outer  $\text{N}=\text{N}$  stretch. This shows that if simulated and experimental bands have the same relative blue shift with decreasing  $x$ , it is possible that the  $\text{C}\equiv\text{O}$  and  $\text{N}=\text{N}$  fundamental vibrations are overlapped.

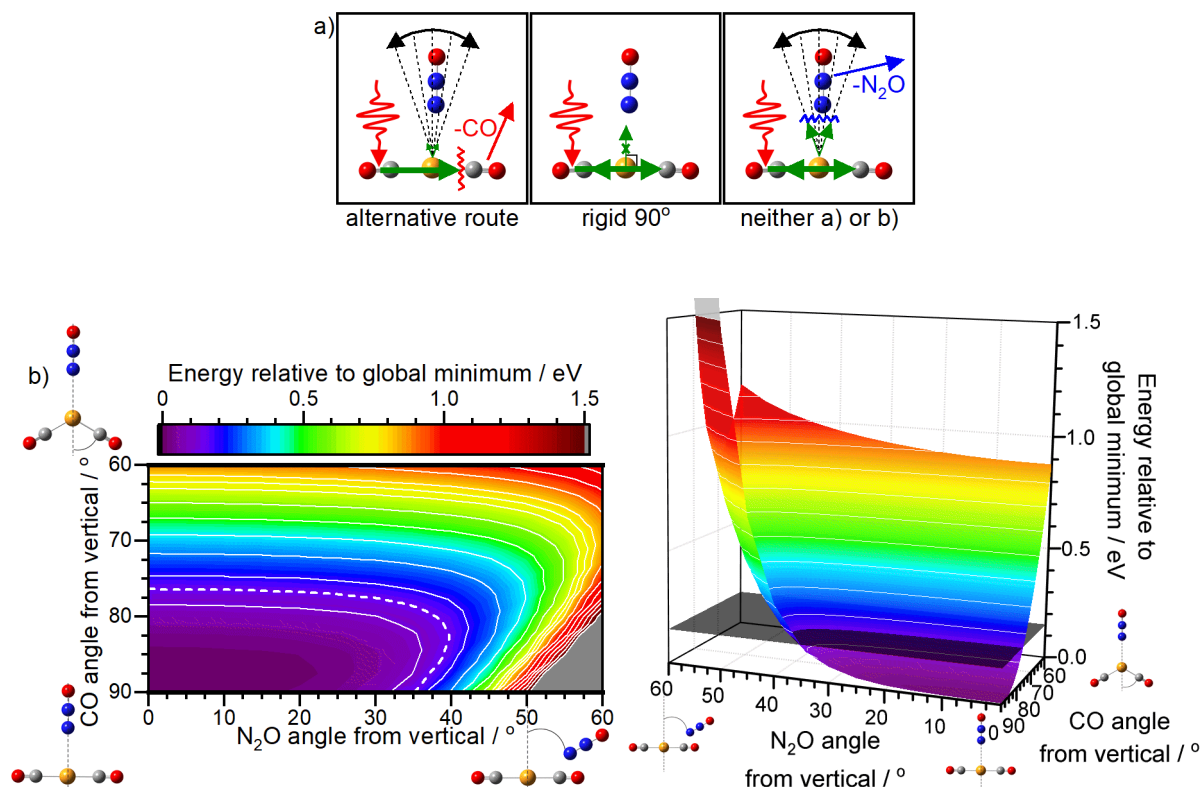


**Figure S8.** a) Factors to consider if the energy flow is hindered geometrically include: whether the preferred route leads to an alternative loss channel, and how flexible the structure is. The geometrically hindered loss channel is conceivably reached if there is no alternate route and there is large amplitude motion. b) The potential energy surface (in 2D and 3D) spanning the coordinates of the N<sub>2</sub>O and CO angles of Au(CO)<sub>2</sub>(N<sub>2</sub>O)<sup>+</sup> from their equilibrium position (3.4, 87.5°). All other coordinates are kept rigid. Note that here the energy is given relative to the electronic energy of this equilibrium position. The dashed line at 0.15 eV indicates the total zero point energy of all intermolecular modes.

To see the signature of a CO absorption in the N<sub>2</sub>O loss channel of Au(CO)<sub>2</sub>(N<sub>2</sub>O)<sup>+</sup>, 0.15 eV from 0.27 eV photon(s) is needed in order to break the Au-N<sub>2</sub>O bond. The energy absorbed spreads over the cluster according to the density of states, but geometric effects could also be prominent. Energy transfer from the C≡O mode to Au--N (O≡C → C--Au → Au--N<sub>2</sub>O) will be hindered by the orthogonal angle, *i.e.*, if an atom is vibrating in the  $0\mathbf{i} + 1\mathbf{j}$  direction it has no component in  $1\mathbf{i} + 0\mathbf{j}$ , and therefore no direct energy transfer. Accordingly, the linear O≡C → C—Au → Au--CO is a highly preferred energy path. For this geometrical reasoning, a signature of N<sub>2</sub>O loss at the C≡O stretch may not be observed if, as shown schematically in Figure S8a, either: i) the preferred route leads to another desorption path (left panel), or ii) the cluster is rigid (central panel). However, neither of these are the case and the situation is more likely demonstrated by the right panel of Figure S8a.

The left panel of Figure S8a is important to consider, because, if followed by fast vibrational predissociation of the Au--CO bond, the relative rates of IVR to Au--C ( $180^\circ$ ) compared with to Au--N ( $90^\circ$ ) could make a significant difference and the energy needed for desorption ( $> \frac{1}{2} h\nu$ ) would not reach Au--N. However, no CO loss is seen due to the strength of the Au--CO bond. The experiment is not designed to measure absolute IVR rates. The IVR timescale is fast (fs-ps timescale) and sufficient energy for fragmentation would be expected to reach Au--N on the experimental timescale.

The flexibility of the cluster is also an important feature, because the direct transfer of energy around a rigid  $90^\circ$  corner is inefficient. However, the structure is not static and large amplitude motion expected, as shown in Figure S8b. Here the colour scale interpolates between energies of rigid single point calculations at  $2.5^\circ$  steps in both angle dimensions. By way of example, bending as far as 0.15 eV is shown in the dashed line. The N<sub>2</sub>O moiety undergoes larger amplitude motion than the CO. N<sub>2</sub>O  $\leftrightarrow$  CO energy flow becomes more likely the further from perpendicular the mutual angle becomes.

For  $x = 1$  clusters, there is a clear signature of the core N<sub>2</sub>O ligand at  $2355\text{ cm}^{-1}$ . Direct N<sub>2</sub>O loss is unlikely due to the high core ligand binding energy. In this case, despite a similar geometry to Au(CO)<sub>2</sub>(N<sub>2</sub>O)<sup>+</sup>, the coupling of an inner Au--N to outer Au--N is much more efficient than inner Au--C to outer Au--N, due to the similarity in Au--N vibrational frequencies. In addition, the photon energy of a core N=N vibration is 7% higher (0.29 eV) and outer N<sub>2</sub>O desorption energy thresholds lower (see Figure S13 later) for  $x = 1$  systems.

## Future isotopologue studies

To confidently assign the singular band in  $x = 1$  and 2 complexes to both  $\text{N}_2\text{O}$  and  $\text{CO}$  molecular vibrations, it would involve using  $^{13}\text{C}$  enriched  $\text{CO}$ . A larger reduced mass would red shift the  $\text{CO}$  band frequency by *ca.*  $50\text{ cm}^{-1}$ , as shown by the simulated spectra in Figure S9, and with a FWHM of *ca.*  $10\text{ cm}^{-1}$  the  $^{13}\text{C}\equiv\text{O}$  absorption (red line) would be distinguishable from the  $\text{N}_2\text{O}$  band (blue line).

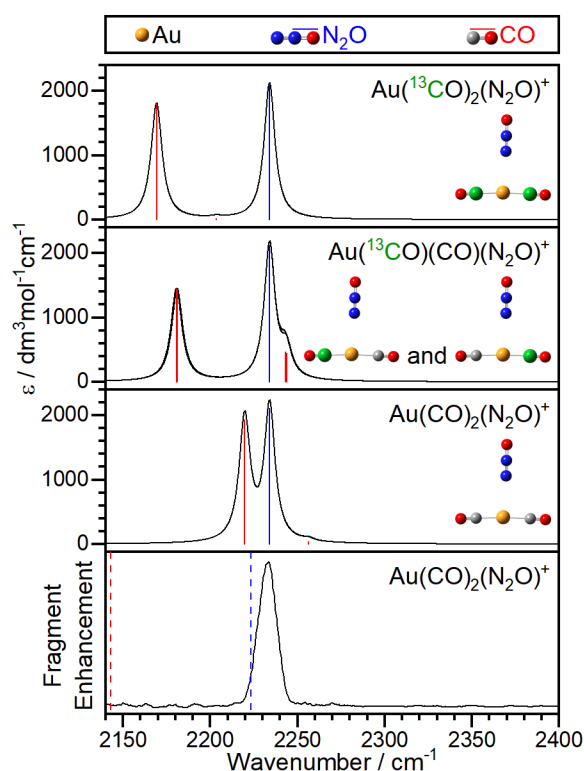


**Figure S9.** Comparison of the IRPD spectrum of  $\text{Au}(\text{CO})_2(\text{N}_2\text{O})^+$  with the simulated IR spectra of the lowest energy isomer (with and without isotopically labelled carbon,  $^{13}\text{C}$ ). The dashed lines indicate the frequency of the  $^{12}\text{C}\equiv\text{O}$  stretch ( $2143.2\text{ cm}^{-1}$ ) and  $\text{N}=\text{N}$  stretch ( $2223.5\text{ cm}^{-1}$ ) vibrations in free  $^{12}\text{CO}$  and  $\text{N}_2\text{O}$ , respectively.<sup>11-12</sup>

## E. Photofragmentation Dynamics and Branching Ratios

Further details and fixed wavenumber time-of-flight spectra associated with Section 3.2 of the main text.

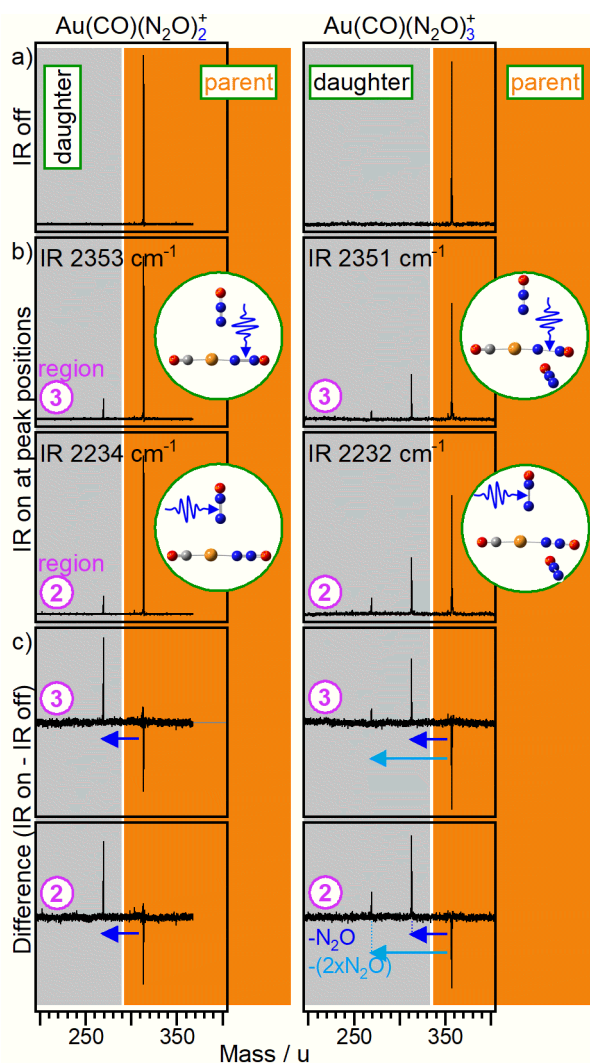


**Figure S10.** Time-of-flight mass spectra of a) mass selected  $\text{Au(CO)(N}_2\text{O)}_y^+$  ( $y = 2,3$ ), and b) IR excited  $\text{Au(CO)(N}_2\text{O)}_y^+$  ( $y = 2,3$ ). The spectral regions (pink numbers) are defined in Table S1, where region 3 is resonant with a core  $\text{N}_2\text{O}$  and region 2 is resonant with an  $\text{N}_2\text{O}$  in the second solvation shell. Mass peaks corresponding to daughter fragments are present in the shaded grey area, whereas parent peaks are in the region shaded orange. c) The difference of a) and b) with depletion and enhancement of signal plotted in the negative and positive directions, respectively. Arrows indicate the mass difference corresponding to the loss of  $\text{N}_2\text{O}$  (dark blue) and loss of  $2 \times \text{N}_2\text{O}$  (light blue).



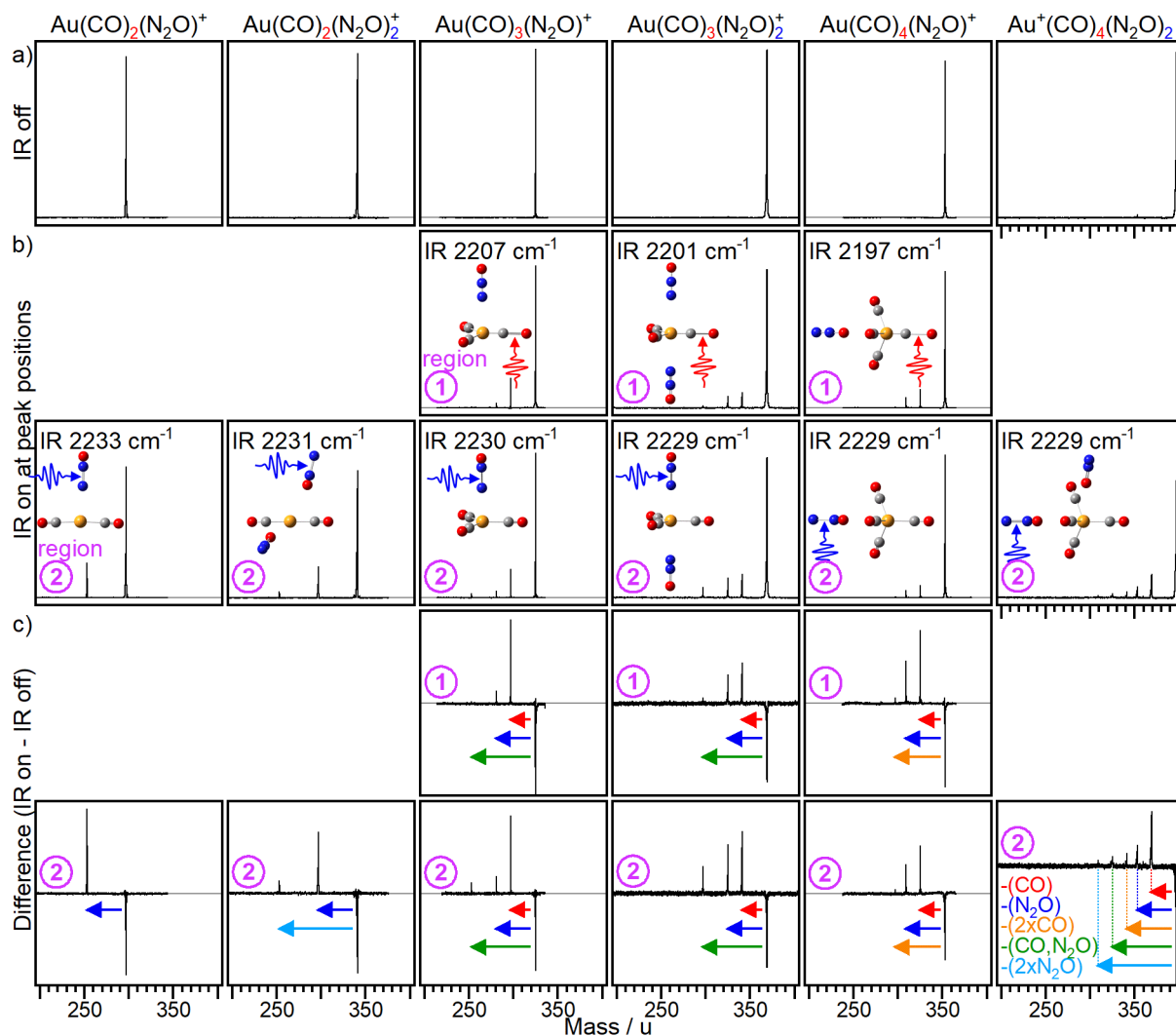


**Figure S11.** Time-of-flight mass spectra of a) mass selected  $\text{Au(CO)}_x(\text{N}_2\text{O})_y^+$  ( $x = 2-4$ ,  $y = 1-2$ ) and b) IR excited  $\text{Au(CO)}_x(\text{N}_2\text{O})_y^+$  ( $x = 2-4$ ,  $y = 1-2$ ). Regions are defined in Table S1. c) The difference of a) and b) with depletion of parent ions and enhancement of daughter fragment ions plotted in the negative and positive directions, respectively. The coloured arrows indicate the fragment lost, as defined in the bottom-right panel.

## Two ligand loss channels

As shown for Figure 9 of the main text but now considering all possible two ligand loss channels. For  $\text{Au}(\text{CO})_3(\text{N}_2\text{O})_2^+$  and  $\text{Au}(\text{CO})_4(\text{N}_2\text{O})^+$ , there are two loss channels with low energy thresholds which are given to the right of the panels in Figure S12. Ligand weighted reasoning can be used to explain the identity of the two ligand loss channels observed,  $-(\text{CO}, -\text{N}_2\text{O})$  from  $\text{Au}(\text{CO})_3(\text{N}_2\text{O})_2^+$  and  $-(2\times\text{CO})$  from  $\text{Au}(\text{CO})_4(\text{N}_2\text{O})^+$ . The weighting is calculated by simply counting all the possible combinations for each two ligand loss channel. For example, for  $-(\text{CO}, \text{N}_2\text{O})$  from  $\text{Au}(\text{CO})_3(\text{N}_2\text{O})_2^+$  each CO can leave with either one of the two  $\text{N}_2\text{O}$  molecules making 6 possible combinations of  $(\text{CO}, \text{N}_2\text{O})$  loss. Whereas for  $-2\times\text{CO}$  and  $-2\times\text{N}_2\text{O}$  there are 3 and 1 possible combinations, respectively. These weightings are given as a ratio to the left of each panel in Figure S12. Two ligand loss is a minor process, therefore, when several have low dissociation thresholds, only the channel with the highest weighting is detected in each case.

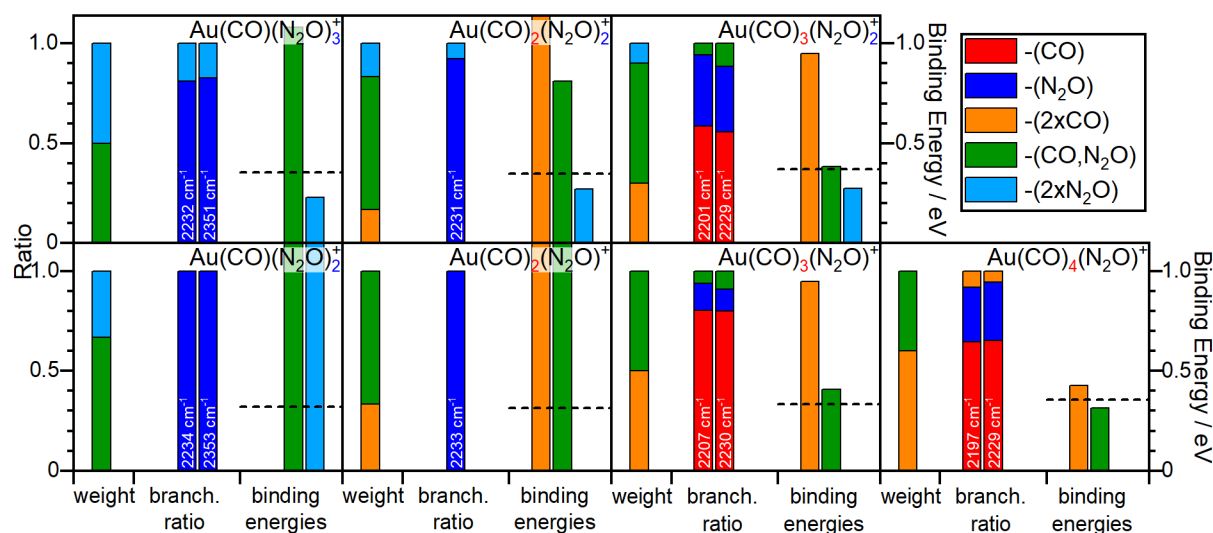


**Figure S12.** Branching ratios from areas of absolute depletion spectra compared with the cluster composition (weight) and relevant binding energies for two ligand loss. In this case the weight is calculated as the number of possible combinations that would achieve the two ligand loss channel. The dashed line indicates the mean internal energy of the complex at 100 K plus a photon energy of 0.27 eV (*i.e.*,  $\langle U_{\text{vib}}(100 \text{ K}) \rangle + h\nu$ ).



## G. Effects of Multiple Photon Absorption

Further to Section 3.4 of the main text and as the first row of Figure 11 but fitting mean data points rather than distributions.

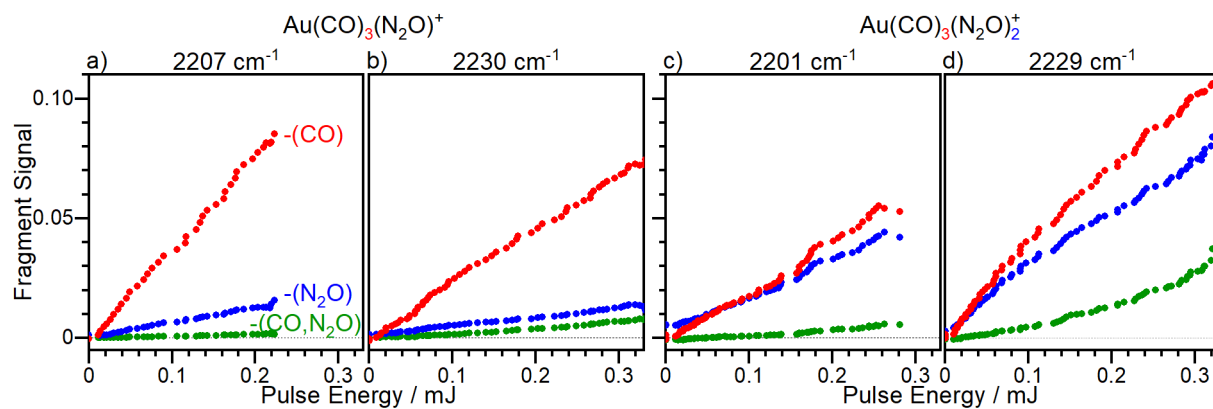


**Figure S14.** Fragment peak signal as a function of infrared laser pulse energy for resonant excitation of  $\text{Au(CO)}_3(\text{N}_2\text{O})_y^+$  ( $y = 1$  and  $2$ ). The intensity of each daughter fragment is normalised to the total intensity of all peaks (parent and daughter fragments) and therefore represents the fragmentation yield,  $\Phi_i(\bar{\nu})$ , as defined in the main text.

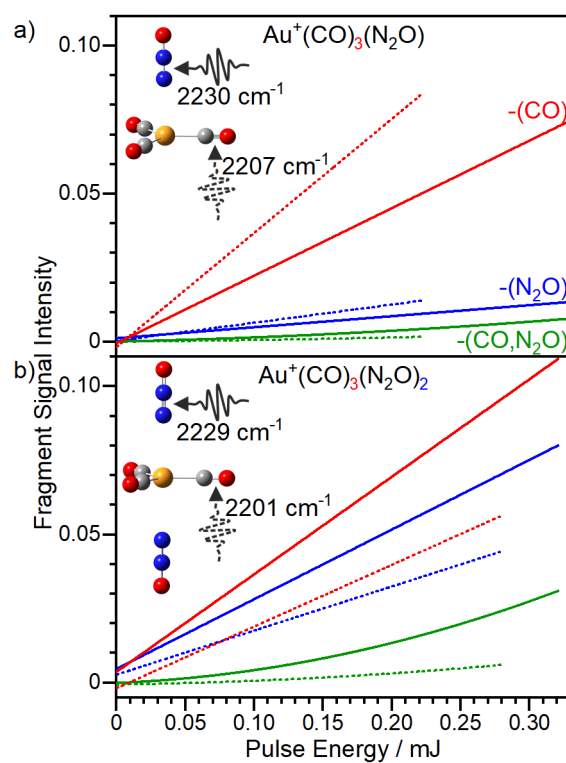


**Figure S15.** Fitted pulse energy dependence of a)  $\text{Au}(\text{CO})_3(\text{N}_2\text{O})^+$  and b)  $\text{Au}(\text{CO})_3(\text{N}_2\text{O})_2^+$  to compare the mode selectivity of the multiple photon character in the  $-(\text{CO}, \text{N}_2\text{O})$  loss channel (green). Solid and dotted lines indicate pumping of  $\text{N}_2\text{O}$  and  $\text{CO}$  modes, respectively. In a) for  $-\text{CO}$  and  $-\text{N}_2\text{O}$  the slope is higher at the 2207  $\text{cm}^{-1}$  band, whereas for  $-(\text{CO}, \text{N}_2\text{O})$  2230  $\text{cm}^{-1}$  is higher.

## H. References:

1. Addicoat, M. A.; Metha, G. F., Kick: constraining a stochastic search procedure with molecular fragments. *J Comput Chem* **2009**, *30*, 57-64.
2. Becke, A. D., Density-functional thermochemistry. III. The role of exact exchange. *J Chem Phys* **1993**, *98* (7), 5648-5652.
3. Perdew, J. P., Density-functional approximation for the correlation energy of the inhomogeneous electron gas. *Phys Rev B* **1986**, *33* (12), 8822-8824.
4. Weigend, F.; Ahlrichs, R., Balanced basis sets of split valence, triple zeta valence and quadruple zeta valence quality for H to Rn: Design and assessment of accuracy. *Phys Chem Chem Phys* **2005**, *7* (18), 3297-305.
5. Weigend, F., Accurate Coulomb-fitting basis sets for H to Rn. *Phys Chem Chem Phys* **2006**, *8*, 1057-65.
6. Andrae, D.; Häußermann, U.; Dolg, M.; Stoll, H.; Preuß, H., Energy-Adjusted Ab Initio Pseudopotentials for the Second and Third Row Transition Elements. *Theor Chim Acta* **1990**, *77*, 123-141.
7. Perdew, J. P.; Tao, J.; Staroverov, V. N.; Scuseria, G. E., Meta-generalized gradient approximation: explanation of a realistic nonempirical density functional. *J Chem Phys* **2004**, *120* (15), 6898-911.
8. Tao, J.; Perdew, J. P.; Staroverov, V. N.; Scuseria, G. E., Climbing the density functional ladder: nonempirical meta-generalized gradient approximation designed for molecules and solids. *Phys Rev Lett* **2003**, *91* (14), 146401.
9. Grimme, S.; Antony, J.; Ehrlich, S.; Krieg, H., A consistent and accurate ab initio parametrization of density functional dispersion correction (DFT-D) for the 94 elements H-Pu. *J Chem Phys* **2010**, *132*, 154104.
10. Grimme, S.; Ehrlich, S.; Goerigk, L., Effect of the damping function in dispersion corrected density functional theory. *J Comput Chem* **2011**, *32* (7), 1456-65.
11. Herzberg, G., *Molecular Spectra and Molecular Structure*. Krieger Publishing Company: Malabar, Florida, 1989; Vol. I. Spectra of Diatomic Molecules.
12. Herzberg, G., *Molecular Spectra and Molecular Structure*. Krieger Publishing Company: Malabar, Florida, 1991; Vol. II. Infrared and Raman Spectra of Polyatomic Molecules.
13. Scott, A. P.; Radom, L., Harmonic Vibrational Frequencies: An Evaluation of Hartree-Fock, Møller-Plesset, Quadratic Configuration Interaction, Density Functional Theory, and Semiempirical Scale Factors. *J Phys Chem-Us* **1996**, *100* (41), 16502-16513.
14. Ricks, A. M.; Reed, Z. E.; Duncan, M. A., Infrared spectroscopy of mass-selected metal carbonyl cations. *J Mol Spectrosc* **2011**, *266* (2), 63-74.
15. Velasquez, J.; Njagic, B.; Gordon, M. S.; Duncan, M. A., IR photodissociation spectroscopy and theory of Au<sup>+</sup>(CO)<sub>n</sub> complexes: nonclassical carbonyls in the gas phase. *J Phys Chem A* **2008**, *112* (9), 1907-13.
16. Cunningham, E. M.; Gentleman, A. S.; Beardsmore, P. W.; Iskra, A.; Mackenzie, S. R., Infrared Signature of Structural Isomers of Gas-Phase M<sup>+</sup>(N<sub>2</sub>O)<sub>n</sub> (M = Cu, Ag, Au) Ion-Molecule Complexes. *J Phys Chem A* **2017**, *121* (40), 7565-7571.
17. Zhou, M.; Andrews, L.; Bauschlicher, C. W., Spectroscopic and theoretical investigations of vibrational frequencies in binary unsaturated transition-metal carbonyl cations, neutrals, and anions. *Chem Rev* **2001**, *101* (7), 1931-61.
18. Willner, H.; Aubke, F., Reaction of carbon monoxide in the super acid HSO<sub>3</sub>F·Au(SO<sub>3</sub>F)<sub>3</sub>, and the gold(I)bis(carbonyl)cation [Au(CO)<sub>2</sub>]<sup>+</sup>. Isolation and characterization of gold(I) carbonyl fluorosulfate, Au(CO)SO<sub>3</sub>F. *Inorg Chem* **1990**, *29* (12), 2195-2200.
19. Willner, H.; Schaebs, J.; Hwang, G.; Mistry, F.; Jones, R.; Trotter, J.; Aubke, F., Bis(carbonyl)gold(I) undecafluorodiantimonate(V), [Au(CO)<sub>2</sub>][Sb<sub>2</sub>F<sub>11</sub>]: synthesis, vibrational, and carbon-13 NMR study and

the molecular structure of bis(acetonitrile)gold(I) hexafluoroantimonate(V),  $[\text{Au}(\text{NCCH}_3)_2][\text{SbF}_6]$ . *J Am Chem Soc* **1992**, *114* (23), 8972-8980.

20. Aubke, F., The generation of unusual noble-metal cations in fluoro acids and super acids, and their spectroscopic properties. *J Fluor Chem* **1995**, *72* (2), 195-201.

21. Liang, B.; Andrews, L., Reactions of Laser-Ablated Ag and Au Atoms with Carbon Monoxide: Matrix Infrared Spectra and Density Functional Calculations on  $\text{Ag}(\text{CO})_n$  ( $n = 2, 3$ ),  $\text{Au}(\text{CO})_n$  ( $n = 1, 2$ ) and  $\text{M}(\text{CO})_n^+$  ( $n = 1-4$ ;  $\text{M} = \text{Ag}, \text{Au}$ ). *J Phys Chem A* **2000**, *104* (40), 9156-9164.

22. Orgel, L. E., 843. Stereochemistry of metals of the B sub-groups. Part I. Ions with filled *d*-electron shells. *J Chem Soc* **1958**, 4186-4190.

23. Gentleman, A. S.; Green, A. E.; Price, D. R.; Cunningham, E. M.; Iskra, A.; Mackenzie, S. R., Infrared Spectroscopy of  $\text{Au}^+(\text{CH}_4)_n$  Complexes and Vibrationally-Enhanced C-H Activation Reactions. *Top Catal* **2018**, *61* (1), 81-91.

24. Li, Y.; Wang, G.; Wang, C.; Zhou, M., Coordination and solvation of the  $\text{Au}^+$  cation: infrared photodissociation spectroscopy of mass-selected  $\text{Au}(\text{H}_2\text{O})_n^+$  ( $n = 1-8$ ) complexes. *J Phys Chem A* **2012**, *116* (44), 10793-801.